Analytica Chimica Acta, Volume 1302, May 2024, Article number 342492
DOI:10.1016/j.aca.2024.342492

Efficient DNA walker guided by ordered cruciform-shaped DNA track for ultrasensitive and rapid electrochemical detection of lead ion

Nuanfei Zhu[1], Kaixuan Wang[1], Dinghui Xiong[1], Jiaxuan Xiao[1], Yibin Deng[2,3*], Zhugen Yang[4], Zhen Zhang[1,2,3*]

[1] School of the Environment and Safety Engineering, Jiangsu University, Zhenjiang 212013, China.

[2] Medical Laboratory Science, the Affiliated Hospital of Youjiang Medical University for Nationalities, Baise 533000, China.

[3] Key Laboratory of Clinical Molecular Diagnosis and Research for High Incidence Diseases in Western Guangxi, Guangxi, 533000, China.

[4] School of Water, Energy, and Environment, Cranfield University, Milton Keynes, MK43 0AL, UK.

*Corresponding author:

Email: dengyb75@163.com; zhangzhen@ujs.edu.cn

Fax: +86-511-88790955

Published by Elsevier. This is the Author Accepted Manuscript issued with: Creative Commons Attribution License (CC:BY 4.0).
The final published version (version of record) is available online at DOI:10.1016/j.aca.2024.342492. Please refer to any applicable publisher terms of use.

ABSTRACT

The rational design of DNA tracks is an effective pathway to guide the autonomous movement and high-efficiency recognition in DNA walkers, showing outstanding advantages for the cascade signal amplification of electrochemical biosensors. However, the uncontrolled distance between two adjacent tracks on the electrode could increase the risk of derailment and interruption of the reaction. Hence, a novel four-way balanced cruciform-shaped DNA track (C-DNT) was designed as a structured pathway to improve the effectiveness and stability of the reaction in DNA walkers. In this work, two kinds of cruciform-shaped DNA were interconnected as a robust structure that could avoid the invalid movement of the designed DNA walker on the electrode. When hairpin H2 was introduced onto the electrode, the strand displacement reaction (SDR) effectively triggered movements of the DNA walker along the cruciform-shaped track while leaving ferrocene (Fc) on the electrode, leading to a significant enhancement of the electrochemical signal. This design enabled the walker to move in an excellent organized and controllable manner, thus enhancing the reaction speed and walking efficiency. Compared to other walkers moving on random tracks, the reaction time of the C-DNT-based DNA walker could be reduced to 20 min. Lead ion (Pb^{2+}) was used as a model target to evaluate the analytical performance of this biosensor, which exhibited a low detection limit of 0.033 pM along with a wide detection ranging from 0.1 pM to 500 nM. This strategy presented a novel concept for designing a high-performance DNA walker-based sensing platform for the detection of contaminants.

***Keywords**:* Biosensor, Electrochemical analysis, DNA walker, Heavy metal, Rapid detection

1. Introduction

DNA walking devices are a series of DNA molecular nanomachines self-assembled according to the strict Watson-Crick base pairing principle [1-3]. The well-designed DNA walkers can precisely regulate the mechanical motion of a nanoscale objective along a desirable route serving as cargo transport, target detection, and signal output [4, 5]. Benefiting from specific structural and functional properties, DNA walkers have been used in the development of many analytical methods, especially showing great potential in electrochemical biosensors[6, 7]. Notably, DNA walker has shown outstanding advantages in cascade signal amplification of electrochemical sensors owing to the autonomous movement and high-efficiency recognition of walking strands and track strands.[8, 9]. It can possess the ability to autonomously traverse a predetermined track at the nanoscale by swinging arms using driving forces [10, 11] such as enzyme/DNAzyme reaction [12-14] and strand displacement reaction (SDR) [15, 16]. Particularly, DNA walker can release a signal molecule at each step, allowing for the accumulation of repetitive steps to achieve significant signal amplification [17, 18].

Usually, the movement of DNA walker is determined by the dynamic reaction between the walking strand and the designated track [19-21]. Hence, the design of DNA track plays a crucial role in guiding the movement of DNA walker, thus facilitating the

effective binding between the walking strand and the DNA substrate. However, some obvious deficiencies hinder the sensing performance of DNA walker-based biosensors. Traditional DNA tracks are generally constructed by randomly distributed single-stranded DNA on the interface, which presents some troubles in dealing with the distance and uniformity of DNA substrates.[22-24]. Recently, some ordered double DNA tracks have been reported to improve the kinetic of the reaction effectively [25, 26]. Although some improvement has been exhibited in reaction kinetic by programming DNA strands into laddered-shape double tracks, but the ununiformed distance between different groups of laddered tracks still had great impact on the risks mentioned in the single tracks. And the isometric spacing in single direction also reduced the walking rate and sensing efficiency in the walking process. Therefore, it is crucial to design an ordered and equidistant DNA track to enhance the controllability and accelerate reaction rates in the construction of electrochemical biosensors.

Herein, to avoid derailment risks and reaction interruption, an ordered DNA track with a four-way balanced cruciform-shaped structure (C-DNT) was proposed for the design of DNA walker in our electrochemical biosensors. Due to the advantages of perfectly equal track spacing and better orderliness, C-DNT could effectively improve the movement efficiency of the DNA walker on the electrode surface. Simultaneously, the cruciform DNA track was designed with optimal track spacing to prevent erratic movements of the walker. This strategy resulted in enhanced movement efficiency of the walker on the electrode surface, finally achieving a rapid and ultra-sensitive

detection for lead ion (Pb^{2+}). As depicted in **Scheme 1A**, equal molar quantities of two cross DNA with different functions self-assembled to form the cruciform-shaped DNA track (C-DNT). As a DNA track, the obtained C-DNT was subsequently modified on Au electrodes through the Au-S bond, while 6-Mercaptohexanol (MCH) was used to block the nonspecific binding sites. The H3 was firstly attached to the C-DNT by complementary base pairing. After its hairpin structure was opened by a specific sequence region of the walker's swing arm sequence, it was served as walking pivot, resulting the exposure of the pre-locked toehold domains for the Fc-labeled hairpin H2. Then, the strand displacement reaction, initiated by the introduction of H2, triggered the movements of the walker on the electrode effectively. This process could facilitate the Ferrocene (Fc) to be brought on the electrode rapidly and efficiently, thereby enhancing the electrochemical signal significantly (**Scheme 1**). Remarkably, in contrast to the previous DNA tracks, this DNA track exhibited uniform and adjustable spacing, allowing the walker to move in an orderly and uniform stepwise manner and achieving the ultra-sensitive Pb^{2+} detection within 20 min.

Scheme 1. Schematic Illustration of the Proposed Electrochemical Biosensor for Pb^{2+} Detection.

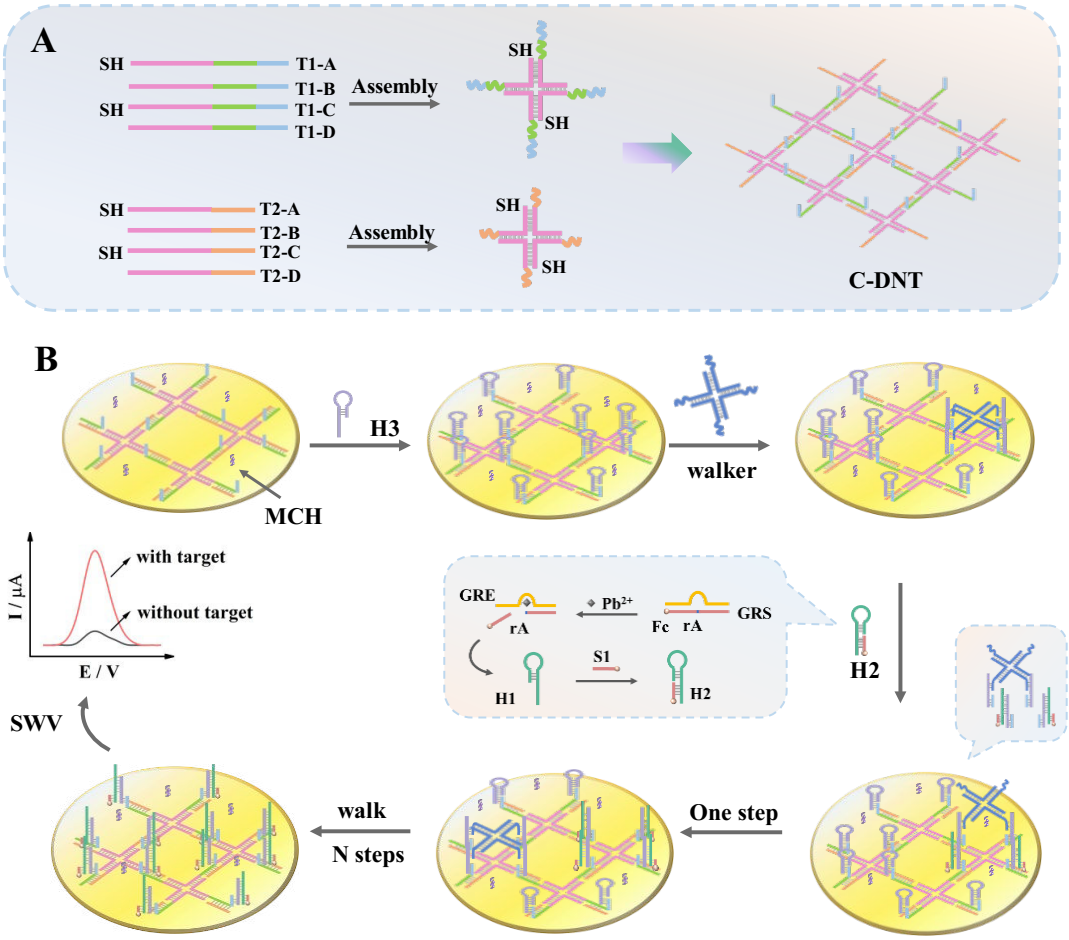

2. Experiment section

2.1. Reagents and Materials

DNA sequences were synthesized and purified by Sangon Biotechnology Company, Ltd. (Shanghai, China), and the corresponding base sequences are listed in **Table S1**. The solutions were prepared using TE buffer to 100 μM and stored at -20 °C. Tris/ethylenediaminetetraacetic acid (EDTA) (TE) buffer and Tris-HCl/magnesium sulfate (TM) buffer were also purchased from Shanghai Sangon Biotechnology Co. Ltd. (Shanghai, China). The hybridization buffer (Tris-HCl buffer, pH 7.4) was comprised

of 20 mM Tris, 140 mM NaCl, and 50 mM $MgCl_2$. The TNaK buffer (40 mM Tris-HCl, pH 7.5, 500 mM NaCl, 10 mM KCl) was used for the preparation of GR-5 DNAzyme. $[Fe(CN)_6]^{3-/4-}$ solution was prepared by combining 5 mM $K_4[Fe(CN)_6]$, 5 mM $K_3[Fe(CN)_6]$, and 0.1 M KCl. The 6-Mercaptohexanol (MCH) was purchased from Meryer Chemical Technology Company, Ltd. Other chemical reagents in this work were of analytical grade. All aqueous solutions were prepared with ultrapure water (Milli-Q, 18 $M\Omega^{-1}$, Merck Millipore).

2.2. Procedure for GR-5 DNAzyme-Pb^{2+} cleavage and H2 construction

The substrate strand (GRS) and enzyme strand [27] at a 1:1 molar ratio were mixed in TNaK buffer, annealed at 95 °C for 5 min, and then slowly cooled to room temperature to form GR-5 DNAzyme (2 μM). Subsequently, the same volume of Pb^{2+} was added to the above product, and 50 min was spent for the cleavage of GRS at 37 °C. Finally, H1 was added to the above mixture to obtain H2.

2.3. Fabrications of DNA walker and DNA track

Four DNA strands (W1, W2, W3, W4) were added to Tris-HCl buffer to get the final concentration of 1 μM. The above mixture was heated for 5 min at 95 °C and gradually cooled down at 25 °C for 2 h to obtain the DNA walker. The fabrication process of the C-DNT was designed according to the previous reference[28]. For the assembly of cruciform DNA, T1, and T2 were respectively prepared by annealing two mixtures off four different single strands (2.0 μM for each one) at 95 °C for 5 min. After cooling to 25 °C for 120 min subsequently, the as-prepared T1 (10 μL, 2.0 μM) and T2 (10μL, 1.0

μM) were mingled for further hybridizing at 35 °C for 120 min to yield the DNA track.

2.4.Construction of the designed biosensor

Firstly, Au electrodes with a diameter of 2 mm (CH Instruments) were cleaned according to the previous protocol [29, 30]. Three microliters of prepared C-DNT solution (1 μM) were then introduced onto the freshly cleaned Au electrode, reacting overnight at room temperature. The MCH (3 μL, 1 mM) was dropped onto the modified electrode and incubated for 30 min at 4 °C. After blocking nonspecific binding sites, 3 μL of H3 (1.4 μM) was subsequently added dropwise onto the electrode for 100 min at room temperature. Ultimately, 3 μL DNA walker and H2 were incubated respectively for the strand displacement reaction.

2.5. Electrochemical section

Cyclic voltammetry (CV), electrochemical impedance spectroscopy (EIS), and square wave voltammetry (SWV) measurements were performed using a CHI Model 660E electrochemical workstation manufactured by CH Instruments, Inc. And a conventional three-electrode system was employed throughout all experiments, including an Au working electrode, an Ag/AgCl reference electrode, and a platinum counter electrode. The $[Fe(CN)_6]^{3-/4-}$ solution was utilized in both CV and EIS electrochemical measurements. The CV was carried out at a scan rate of 100 mV/s over a potential measurement range of -0.2 to 0.6 V. The EIS was recorded by a frequency range from 10^{-1} to 10^{5} Hz with an amplitude of 5 mV. The SWV measurement was implemented in a PBS solution with the following parameters: a potential ranging from

-0.2 to 0.6 V, a potential increment of 4 mV, an amplitude width of 25 mV, and a frequency of 50 Hz. Each measurement was repeated at least three times.

3. Results And Discussion

3.1. Characterization of the Proposed Biosensor

Firstly, the native polyacrylamide gel electrophoresis (PAGE) was employed to verify the formation of the hairpin H2 and the cleaving function of the DNAzyme (**Fig. 1A**). In lane 3, the mixture of M1 and M2 showed a bright band with slower migration, implying the formation of the DNAzyme duplex. In the presence of Pb^{2+}, there were two bands appeared in lane 4, which indicated the successful cleavage of DNAzyme and the release of single-strand S1. After the addition of the cleaved DNAzyme to H1, a slower band was observed in lane 6, demonstrating the desirable hybridization of H2. Then, the fluorescence spectra were performed to further prove the cleavage of DNAzyme. As shown in **Fig. 1B**, the fluorescence intensity of the DNAzyme duplex increased significantly when Pb^{2+} existed, proving that the DNAzyme was successfully cleaved by Pb^{2+}. Moreover, the assembly of the DNA walker and C-DNT were also illustrated by agarose gel electrophoresis (AGE). In **Fig. 1C**, lane 1 to 4 and lane 6 to 9 respectively showed the step-by-step fabrication of cruciform DNA T1 and T2. The mixture of two cruciform DNA showed a band with the slowest electrophoretic mobility in lane 10, suggesting that the C-DNT was formed successfully. Besides, the result of atomic force microscopy (AFM) was presented to further characterize this designed DNA track. As depicted in **Fig. 1D**, there were many evenly distributed DNA circles

with typical morphology of DNA strands in the AFM image, which indicated that the C-DNT was synthesized successfully. Finally, the AGE in **Fig. S1** showed the stepwise fabrication of the DNA walker, in which a clear band with the slowest migration rate was observed in lane 4. These above results demonstrated that the proposed DNA walker and track were generated successfully.

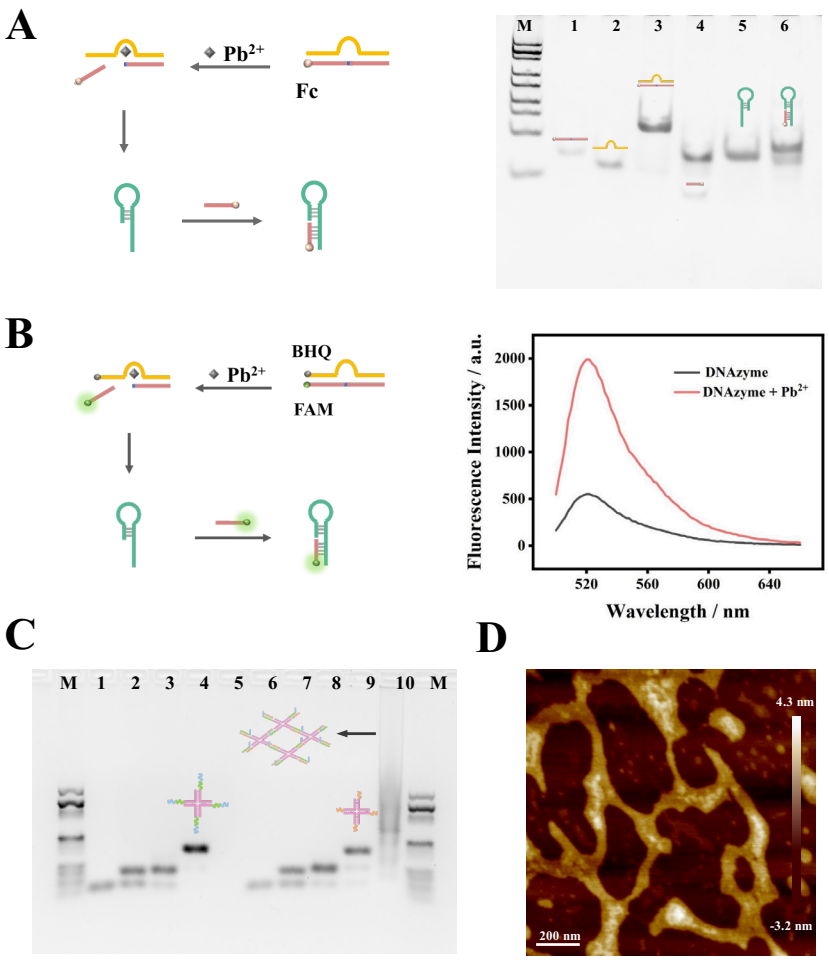

Fig. 1. Characterization of the proposed biosensor. (A) Diagrammatic sketch and PAGE characterization of the hairpin H2 and the cleaving of the Pb^{2+}-dependent DNAzyme. (B) Fluorescence assay of DNAzyme cleavage in the absence and presence of 100 nM Pb^{2+}. (C) AGE characterization of the stepwise assembly of C-DNT. (D) AFM of the track.

3.2. Stepwise Modification on the Electrode

CV and EIS measurements were performed to verify the construction of this electrochemical biosensor for Pb^{2+} detection on the electrode. As illustrated in **Fig. 2A**, curve a represented the peak current generated by the bare Au electrode in the $[Fe(CN)_6]^{3-/4-}$ solution. Then an obvious decline in current was observed after the modification of MCH (curve b) because the electron transfer was hindered. When the C-DNT, H3, DNA walker, and H2 (represented by curve c, d, e, and f) were added on the electrode sequentially, the corresponding electrochemical signals decreased accordingly along with the increasing repulsion between $[Fe(CN)_6]^{3-/4-}$ and the negatively charged DNA.

Furthermore, EIS results were also utilized to prove the successful fabrication of this biosensor in **Fig. 2B**. The resistance of MCH/ Au (curve b) was much bigger than that of bare Au electrode (curve a), which was ascribed to the increase in Ret value caused by MCH. Subsequently, the Ret value increased gradually with the introduction of the C-DNT, H3, DNA walker, and H2 (curve c, d, e, and f). These EIS results have good agreement with that in the CV management, suggesting the effective modification of the biosensor on the electrode.

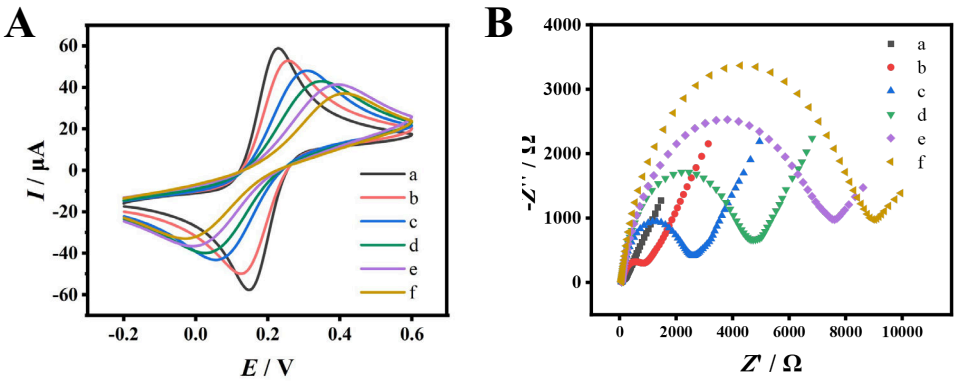

Fig. 2. Characterization of stepwise modification on the electrode. (A) CV and (B) EIS response of (a) bare Au electrode, (b) C-DNT/Au, (c) MCH/C-DNT/Au, (d) H3/MCH/C-DNT/Au, (e) walker/H3/MCH/C-DNT/Au, and (f) H2/walker/H3/MCH/C-DNT/Au.

3.3. Feasibility of the Electrochemical Biosensor

To demonstrate the feasibility of the proposed electrochemical biosensor, SWV was performed for further verification. In **Fig. 3**, after the immobilization of C-DNT on the electrode through the Au−S bond, a negligible SWV signal (curve a) was observed in the absence of DNA walker and hairpin H2, illustrating this sensing strategy possesses a lower background. After adding DNA walker, the signal was almost unchanged (curve b). When the walker and H2 were both introduced (curve c), the peak current increased significantly because the signal label Fc was carried by H2, proving the successful moving of the DNA walker. These results indicated that the proposed biosensor was very suitable for Pb^{2+} detection.

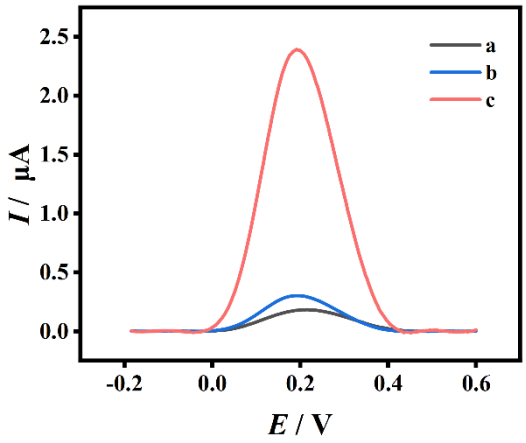

Fig. 3. Feasibility detection of the proposed electrochemical biosensor. SWV signals of (a) H3/ MCH/ C-DNT/ Au, (b) walker/ H3/ MCH/ C-DNT/ Au, (c) H2/ walker/ H3/ MCH/ C-DNT/ Au.

3.4. Optimization of Reaction Conditions

Several experimental conditions that could potentially affect the method were optimized to get the biosensor with a better analytical performance. Firstly, the cleavage time of Pb^{2+} to the DNAzyme is one of the most important factors influencing the detection sensitivity. According to **Fig. S2A**, the peak current increased over time and the maximum SWV value was gained after 50 min, then decreased gradually. Therefore, 50 min was chosen as the optimized time for the Pb^{2+} cleavage. Also, the hybridization time between H1 and cleaved DNAzyme is associated with the number of the Fc modification. In **Fig. S2B**, the current went up with the increase of the hybridization time and then remained stable after 40 min. Hence, the optimized reaction time between H1 and cleaved DNAzyme was 40 min. For the concentration of C-DNT at the electrode (**Fig. S2C**), the SWV current maintained an increasing trend until the concentration exceeded 1 μM, which indicates that 1 μM was the optimal concentration of C-DNT.

And as shown in **Fig. S2D**, the concentration of H3 also followed the same trend as C-DNT up to 1.4 μM, so a concentration of 1.4 μM was chosen for the H3. Moreover, the reaction time of H3 would influence the walking efficiency of DNA walker on the electrode, which was also indispensable to enhance the sensitivity of this sensor. As depicted in **Fig. S2E**, it can be seen that the SWV current decreased when the reaction time exceeded 100 min, illustrating that the most suitable reaction time of H3 was 100 min. In addition, H2 could effectively drive the DNA walker to move through the toehold-mediated strand displacement reaction, bringing the labeled Fc close to the electrode surface and thus enhancing the SWV signal. From **Fig. S2F,** the current response increased significantly from 5 to 20 min, followed by a stable platform at 20 min. Consequently, 20 min was deemed optimal for the H2 reaction.

3.5.Performance Comparison of C-DNT-based DNA Walker in This Strategy

Comparative experiments were utilized to verify the superior performance of the C-DNT-based DNA walker in contrast to conventional DNA walkers that depended on random DNA tracks. The schematic illustration of three biosensors were shown in **Fig. 4A** (stochastic single track-based biosensor as type a, ordered double track-based biosensor as type b, and ordered cruciform DNA track as type c). Firstly, three different types of based biosensors were evaluated under identical reaction conditions (60 min) to assess the conversion efficiency of the electrochemical signal. **Table 1** showed the results from the evaluation of three types of biosensors. It revealed that the stochastic single-track-based biosensor (type a) exhibited the highest background signal and the

lowest walking efficiency, together with a conversion efficiency of 52.1%. Following that, the ordered double track-based biosensor (type b, 78.4%) exhibited the second-highest background signal and walking efficiency. Remarkably, a significant improvement was observed when the structural unit of the proposed biosensors transitioned from a disordered DNA track to an ordered cruciform DNA track (type c) anchored on the electrode surface. This modification highlighted the advantages of this strategy including a substantial decrease in the background signal and a rapid increase in walking efficiency (an impressive 87%). Moreover, the kinetics of the three types of DNA track mentioned above were compared, and the corresponding kinetic data were provided in **Supporting Information**. As depicted in **Fig. 4B**, the proposed type c (curve c) achieved saturation within 20 min whereas the time of type b to remain stable was 40 min. On the contrary, type a (curve a) exhibited a quite slow SWV signal change and could not reach a saturation platform within 2h. Finally, the relationships between the current intensity and reaction time of the three types were further calculated in **Fig. 4C**. The results showed that the maximum rate of type c (7.85 μA/h) was at least 6-fold higher than that of type a (1.18 μA/h) and faster than that of type b (4.39 μA/h). As described in the results, the DNA walker based on a well-designed cruciform DNA track exhibited a significantly higher walking efficiency than that conventional DNA walkers relying on randomly distributed DNA tracks and double tracks. The most probable reason was that the ordered cruciform track had a fully controllable spacing compared to those two types of DNA tracks, which could address the problem of DNA walker

derailment and response disruption, enabling the DNA walker to move with higher directionality and controllability.

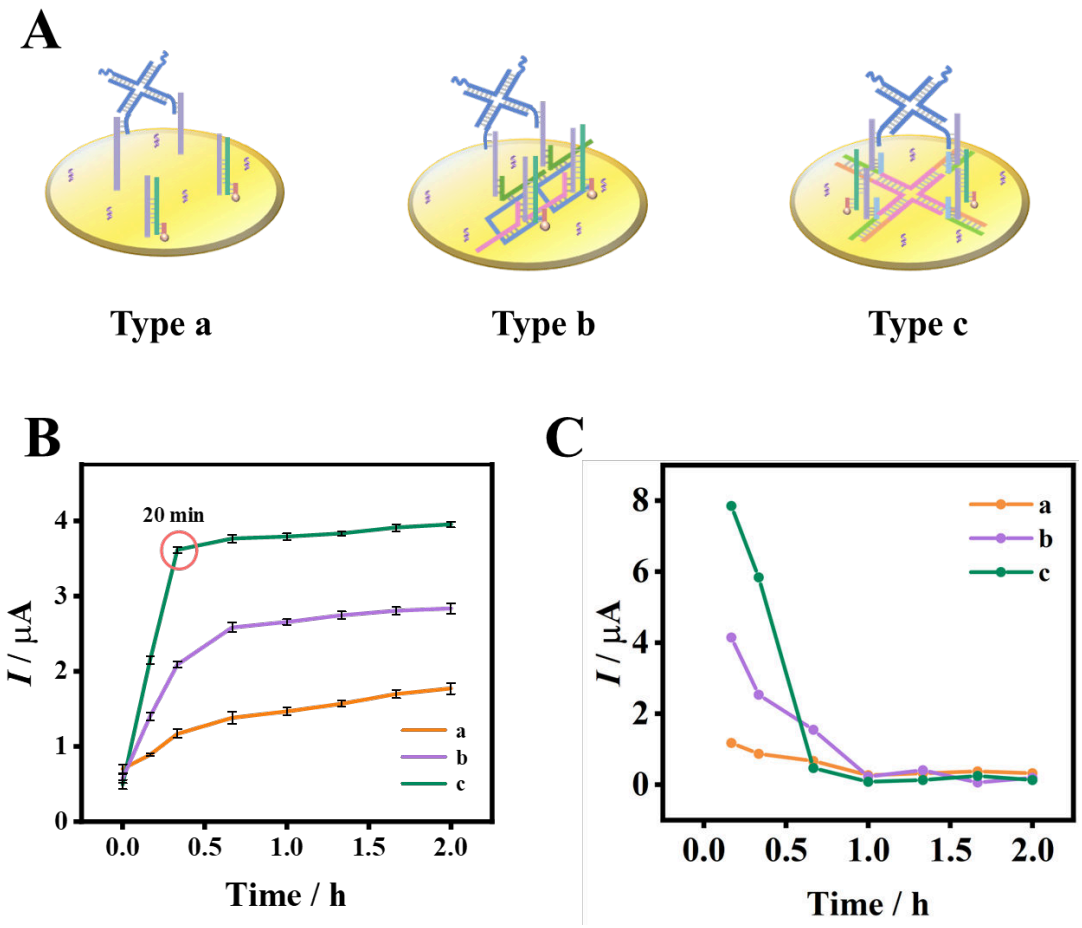

Fig. 4. Performance comparison of three types of biosensors. (A) Schematic illustration of stochastic single track-based biosensor (as type a), double track-based biosensor (as type b), and ordered cruciform DNA track-based biosensor (type c). (B) Reaction kinetics of three biosensors in the presence of 100 nM Pb^{2+}. (C) Walking rates of three biosensors in the presence of 100 nM Pb^{2+}.

Table 1. Comparison of the walking efficiency of three biosensors under the same conditions

Type	I_0 /μA	I_{v60} /μA	ΔI /μA	Efficiency, %
a	0.702	1.467	1.09	52.1%
b	0.574	2.656	2.082	78.4%
c	0.492	3.792	3.3	87 %

3.6. Analytical performance of the proposed biosensor

Under the optimized parameters, the analytical performance of the proposed sensing platform was evaluated by SWV response with different concentrations of Pb^{2+}. As shown in **Fig. 5A**, the SWV response of Fc increased with the concentration of Pb^{2+} increased from 0.1 pM to 500 nM. The **Fig. 5B** depicted a satisfactory linear relationship between the SWV peak current of the Fc and the logarithm of Pb^{2+} concentration. The regression equation was: $I = 0.487 \log c + 2.389$ ($R^2 = 0.981$) with a low detection limit (LOD) of 0.033 pM. Hence, this novel DNA track-based DNA walker showed excellent analytical performance compared with previous reports for Pb^{2+} detection (**Table 2**).

To evaluate the selectivity of the biosensor, 10 different metal ions were used under the optimized experimental conditions, including Cu^{2+}, Hg^{2+}, Mn^{2+}, Fe^{2+}, Fe^{3+}, Ca^{2+}, Cd^{2+}, Co^{2+}, $Ba^{2+,}$ and Ni^{2+}. As depicted in **Fig. 6A**, the SWV current peak of the target Pb^{2+} exhibited a substantial increase compared to that of interfering ions. Furthermore, the difference in the current peaks between Pb^{2+} and the mixture of all ions was almost

negligible, emphasizing that this developed biosensor possessed an exceptional selectivity and anti-interference capability for the accurate detection of Pb^{2+}. Furthermore, the stability of the detection platform was continuously monitored by storing the biosensor at 4°C and conducting the same test every five days. As shown in **Fig. 6B**, the electrochemical signal in the last day could be maintained at 97% of the initial value, showing an acceptable stability of the sensing platform. From **Fig. 6C** and **6D**, the reproducibility of this biosensor was assessed through repetitive measurements. Under the same experimental condition, the relative standard deviation (RSD) of the same batch (intra-assays) was 2.53% and that of six different batches (inter-assays) of biosensors was tested at 4.32%, demonstrating the good reproducibility of this biosensor.

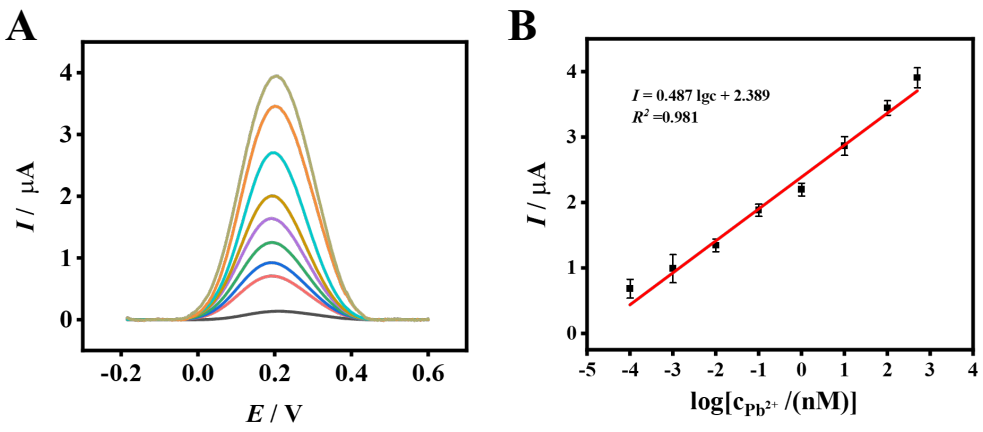

Fig. 5. (A) SWV responses of constructed DNA biosensor to different concentrations of Pb^{2+} (from a to i: 0, 0.1 pM, 1 pM, 10 pM, 100 pM, 1 nM, 10 nM, 100 nM, and 500 nM). (B) Calibration plot of SWV peak current versus the logarithm of Pb^{2+} concentration.

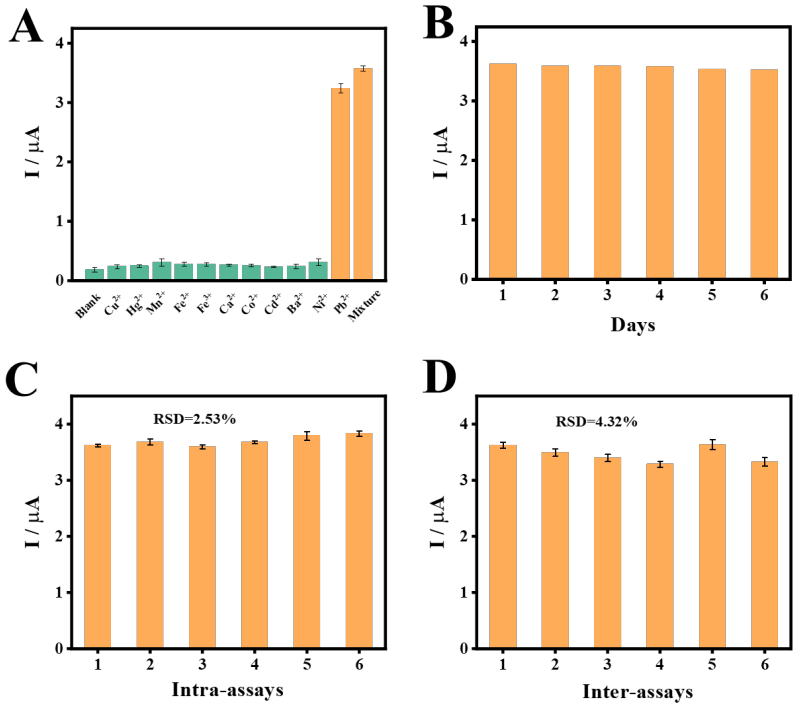

Fig. 6. (A) Specificity and (B) stability of the designed biosensor. Reproducibility of the biosensor (C) in the same batch (intra-assays) and (D) in six different batches (inter-assays).

Table 2. Comparison of the proposed DNA walker-based Biosensor with Previous Reports for Pb^{2+} Detection

Detection method	Linear range	Detection limit	Refs
Colorimetric	2.0 to 10.0 μM	0.2 μM	[31]
Colorimetric	0.8 nM to 2500 nM	0.54 nM	[32]
Colorimetric	10 nM to 1.0 μM	4.3 nM	[33]
Fluorescence	50 to 600 pM	31 pM	[34]
Fluorescence	5 nM to 25 μM	5 nM	[35]
Fluorescence	1 pM to 100 nM	0.2 pM	[36]
ACV	0.2 pM to 100 nM	0.048 pM	[37]
SWASV	0.48 nM to 0.97 μM	0.0145 nM	[38]
DPV	1.0 pM to 2.0 nM	0.98 pM	[39]
DPV	0.1 to 80 ng mL^{-1}	0.05 ng mL^{-1}	[40]
DPV	1 pM to 100 nM	0.34 pM	[41]
SWV	50 pM to 5 μM	5 pM	[42]
SWV	**0.1 pM to 500 nM**	**0.033 pM**	**This work**

3.7. Detection of Pb^{2+} in real samples

To assess the practicability of this proposed electrochemical biosensor in real applications, recovery experiments were carried out through standard addition methods. Various concentrations of Pb^{2+} (0.5, 50, 100, and 250 nM) were introduced into real samples (tap water and river water), and the corresponding results were shown in **Table S3**. The recoveries ranged from 97.8% to 104.7% respectively, demonstrating that the method could be utilized for Pb^{2+} detection accurately and reliably.

4. Conclusion

In summary, a quadrivalent cruciform DNA track (C-DNT) was developed to facilitate the orderly movement of the q-walker, ensuring high walking efficiency for rapid and sensitive Pb^{2+} detection. The better orderliness and equidistance of the

quadrivalent cruciform DNA track enabled the DNA walker to move with high directionality and controllability, while reducing the risk of DNA walker derailment and further enhancing walking efficiency. This biosensor had a satisfactory detection range from 0.1 pM to 500 nM with a detection limit (LOD) of 0.033 pM. At the same time, good selectivity, repeatability, and stability were performed for the detection of the target Pb^{2+}. In conclusion, a novel approach for enhancing DNA walking efficiency and DNA track design was introduced to set a new reference in the relevant field. Moreover, the proposed strategy had significant potential for applications in contaminant detection.

Acknowledgements

This work was supported by the National Natural Science Foundation of China (Grants No. 22176075 and 21876067), the special scientific research project of School of Emergency Management, Jiangsu University (KY-C-02, KY-D-06), the Student Scientific Research Project from Jiangsu University (Grant No. 22A105) and the Jiangsu Collaborative Innovation Center of Technology and Material of Water Treatment.

References

[1] C. Ashworth, DNA nanotechnology: Building big with DNA bricks, Nature Reviews Materials, 3 (2018) 17092.

[2] M. Xu, D. Tang, Recent advances in DNA walker machines and their applications coupled with signal amplification strategies: A critical review, Analytica Chimica Acta, 1171 (2021) 338523.

[3] Y. Guo, S. Liu, H. Yang, P. Wang, Q. Feng, Proximity binding-triggered multipedal DNA walker for the electrochemiluminescence detection of telomerase activity, Analytica Chimica Acta, 1144 (2021) 68-75.

[4] T.-G. Cha, J. Pan, H. Chen, H.N. Robinson, X. Li, C. Mao, J.H. Choi, Design Principles of DNA Enzyme-Based Walkers: Translocation Kinetics and Photoregulation, Journal of the American Chemical Society, 137 (2015) 9429-9437.

[5] D. Wang, C. Vietz, T. Schröder, G. Acuna, B. Lalkens, P. Tinnefeld, A DNA Walker as a Fluorescence Signal Amplifier, Nano Letters, 17 (2017) 5368-5374.

[6] L. Yang, H. Guo, Q. Gao, T. Hou, J. Zhang, X. Liu, F. Li, Integrating Reliable Pt–S Bond-Mediated 3D DNA Nanomachine with Magnetic Separation in a Homogeneous Electrochemical Strategy for Exosomal MicroRNA Detection with Low Background and High Sensitivity, Analytical Chemistry, 95 (2023) 17834-17842.

[7] X. Liu, J. Xiang, H. Cheng, Y. Wang, F. Li, Engineering Multipedal DNA Walker on Paper for Sensitive Electrochemical Detection of Plant MicroRNA, 40 (2022) 2808-2814.

[8] Y. Gong, M. Fu, L. Li, Y. Yin, Q. Tang, W. Zhou, G. Zhang, X. Liao, F. Gao, DNAzyme-driven tripedal DNA walker mediated signal-on and label-free for electrochemical detection of α-synuclein oligomers, Sensors and Actuators B: Chemical, 378 (2023).

[9] T. Yan, L. Zhu, H. Ju, J. Lei, DNA-Walker-Induced Allosteric Switch for Tandem Signal Amplification with Palladium Nanoparticles/Metal–Organic Framework Tags in Electrochemical Biosensing, Analytical Chemistry, 90 (2018) 14493-14499.

[10] N. Liao, M.C. Pan, L. Wang, F. Yang, R. Yuan, Y. Zhuo, Swing Arm Location-Controllable DNA Walker for Electrochemiluminescence Biosensing, Anal Chem, 93 (2021) 4051-4058.

[11] J. Liu, L.Y. Ye, Y. Zhang, H. Yang, L. Zhou, E. Luo, J. Lei, Nonenzymatic Target-Driven DNA Nanomachine for Monitoring Malathion Contamination in Living Cells and Bioaccumulation in Foods, Anal Chem, 94 (2022) 5667-5673.

[12] L. Zhu, Q. Liu, B. Yang, H. Ju, J. Lei, Pixel Counting of Fluorescence Spots

Triggered by DNA Walkers for Ultrasensitive Quantification of Nucleic Acid, Anal Chem, 90 (2018) 6357-6361.

[13] X. Qu, D. Zhu, G. Yao, S. Su, J. Chao, H. Liu, X. Zuo, L. Wang, J. Shi, L. Wang, W. Huang, H. Pei, C. Fan, An Exonuclease III-Powered, On-Particle Stochastic DNA Walker, Angew Chem Int Ed Engl, 56 (2017) 1855-1858.

[14] H. Gan, J. Wu, H. Ju, Proximity hybridization-induced on particle DNA walker for ultrasensitive protein detection, Anal Chim Acta, 1074 (2019) 142-149.

[15] Y. Zhang, J.H. Li, X.L. Zhang, H.J. Wang, R. Yuan, Y.Q. Chai, Aluminum(III)-Based Organic Nanofibrous Gels as an Aggregation-Induced Electrochemiluminescence Emitter Combined with a Rigid Triplex DNA Walker as a Signal Magnifier for Ultrasensitive DNA Assay, Anal Chem, 95 (2023) 1686-1693.

[16] M. Oishi, K. Saito, Simple Single-Legged DNA Walkers at Diffusion-Limited Nanointerfaces of Gold Nanoparticles Driven by a DNA Circuit Mechanism, ACS Nano, 14 (2020) 3477-3489.

[17] L. Zhang, X. Liu, X. Xu, N. Zhang, W. Jiang, A bipedal-unequivalent three-dimensional DNA walker and its biosensing application, Sensors and Actuators B: Chemical, 327 (2021).

[18] J. Mao, X. Chen, H. Xu, X. Xu, DNAzyme-driven DNA walker biosensor for amplified electrochemical detection of T4 polynucleotide kinase activity and inhibition, Journal of Electroanalytical Chemistry, 874 (2020).

[19] L. Song, Y. Zhuge, X. Zuo, M. Li, F. Wang, DNA Walkers for Biosensing

Development, Advanced Science, 9 (2022).

[20] M. Qing, S. Xie, W. Cai, D. Tang, Y. Tang, J. Zhang, R. Yuan, Click Chemistry Reaction-Triggered 3D DNA Walking Machine for Sensitive Electrochemical Detection of Copper Ion, Analytical Chemistry, 90 (2018) 11439-11445.

[21] Y. Chang, Z. Wu, Q. Sun, Y. Zhuo, Y. Chai, R. Yuan, Simply Constructed and Highly Efficient Classified Cargo-Discharge DNA Robot: A DNA Walking Nanomachine Platform for Ultrasensitive Multiplexed Sensing, Analytical Chemistry, 91 (2019) 8123-8128.

[22] Y. Wang, J. Quan, J. Zhang, K. Huang, X. Wang, H. Jiang, DNA walker induced "signal off" electrochemical cytosensor strategy for ultrasensitive detection of tumor cells, Sensors and Actuators B: Chemical, 366 (2022) 132021.

[23] Y. Wang, Y. Wang, S. Liu, W. Sun, M. Zhang, L. Jiang, M. Li, J. Yu, J. Huang, Toehold-mediated DNA strand displacement-driven super-fast tripedal DNA walker for ultrasensitive and label-free electrochemical detection of ochratoxin A, Analytica Chimica Acta, 1143 (2021) 21-30.

[24] S. Lei, L. Xu, Z. Liu, L. Zou, G. Li, B. Ye, An enzyme-free and label-free signal-on aptasensor based on DNAzyme-driven DNA walker strategy, Analytica Chimica Acta, 1081 (2019) 59-64.

[25] H. Yang, H. Shen, A. Qileng, G. Cui, Z. Liang, Y. Liu, W. Liu, Well-Aligned Track-Accelerated Tripedal DNA Walker for Photoelectrochemical Recognition of Dual-miRNAs Based on Molecular Logic Gates, Anal Chem, 95 (2023) 5764-5772.

[26] T. Yao, L. Kong, Y. Liu, H. Li, R. Yuan, Y. Chai, Highly Efficient Quadruped DNA Walker Guided by Ordered DNA Tracks for Rapid and Ultrasensitive Electrochemical Detection of miRNA-21, Anal Chem, 94 (2022) 12256-12262.

[27] M. Mazumdar, D.C. Bellinger, M. Gregas, K. Abanilla, J. Bacic, H.L. Needleman, Low-level environmental lead exposure in childhood and adult intellectual function: a follow-up study, Environmental Health, 10 (2011) 24.

[28] Y. Zhang, J. Zhao, G. Yang, Y. He, S. Chen, R. Yuan, Ultrasensitive Detection of Amyloid beta Oligomers Based on the "DD-A" FRET Binary Probes and Quadrivalent Cruciform DNA Nanostructure-Mediated Cascaded Amplifier, ACS Appl Mater Interfaces, 13 (2021) 32013-32021.

[29] J. Zhang, S. Song, L. Wang, D. Pan, C. Fan, A gold nanoparticle-based chronocoulometric DNA sensor for amplified detection of DNA, Nature Protocols, 2 (2007) 2888-2895.

[30] R. Lao, S. Song, H. Wu, L. Wang, Z. Zhang, L. He, C. Fan, Electrochemical Interrogation of DNA Monolayers on Gold Surfaces, Analytical Chemistry, 77 (2005) 6475-6480.

[31] C. Dong, X. Ma, N. Qiu, Y. Zhang, A. Wu, An ultra-sensitive colorimetric sensor based on smartphone for pyrophosphate determination, Sensors and Actuators B: Chemical, 329 (2021) 129066.

[32] S. Xu, S. Wang, L. Guo, Y. Tong, L. Wu, X. Huang, Nanozyme-catalysed CRISPR-Cas12a system for the preamplification-free colorimetric detection of lead ion,

Analytica Chimica Acta, 1243 (2023) 340827.

[33] Y.-J. Lan, Y.-W. Lin, A non-aggregation colorimetric method for trace lead(ii) ions based on the leaching of gold nanorods, Analytical Methods, 6 (2014) 7234-7242.

[34] X.-L. Li, H. Jiang, L. Zhao, T.s. Song, J.j. Xie, Self-powered DNA nanomachines for fluorescence detection of lead, Microchimica Acta, 190 (2023) 99.

[35] J. Zhou, M. Qing, Y. Ling, L. Wang, N.B. Li, H.Q. Luo, Double-stranded DNA nanobridge enhanced fluorescence of crystal violet/G-quadruplex complex for detection of lead ions and crystal violet, Sensors and Actuators B: Chemical, 340 (2021).

[36] J. Chen, M. Chen, H. Tong, F. Wu, Y. Liu, C. Liu, Fluorescence biosensor for ultrasensitive detection of the available lead based on target biorecognition-induced DNA cyclic assembly, Sci Total Environ, 905 (2023) 167253.

[37] W. Cai, S. Xie, J. Zhang, D. Tang, Y. Tang, Immobilized-free miniaturized electrochemical sensing system for Pb(2+) detection based on dual Pb(2+)-DNAzyme assistant feedback amplification strategy, Biosens Bioelectron, 117 (2018) 312-318.

[38] N. Qiu, Y. Liu, R. Guo, A novel sensitive electrochemical sensor for lead ion based on three-dimensional graphene/sodium dodecyl benzene sulfonate hemimicelle nanocomposites, Electrochimica Acta, 212 (2016) 147-154.

[39] F. Gao, F. Zhan, S. Li, P. Antwi-Mensah, L. Niu, Q. Wang, Dual signal-based electrochemical aptasensor for simultaneous detection of Lead(II) and Mercury(II) in environmental water samples, Biosens Bioelectron, 209 (2022) 114280.

[40] Z. Dahaghin, P.A. Kilmartin, H.Z. Mousavi, Novel ion imprinted polymer

electrochemical sensor for the selective detection of lead(II), Food Chem, 303 (2020) 125374.

[41] Q. Zhou, Y. Lin, Y. Lin, Q. Wei, G. Chen, D. Tang, Highly sensitive electrochemical sensing platform for lead ion based on synergetic catalysis of DNAzyme and Au-Pd porous bimetallic nanostructures, Biosens Bioelectron, 78 (2016) 236-243.

[42] X. Zhang, X. Huang, Y. Xu, X. Wang, Z. Guo, X. Huang, Z. Li, J. Shi, X. Zou, Single-step electrochemical sensing of ppt-level lead in leaf vegetables based on peroxidase-mimicking metal-organic framework, Biosens Bioelectron, 168 (2020) 112544.

Cranfield University

CERES Research Repository **https://dspace.lib.cranfield.ac.uk/**

School of Water, Energy and Environment (SWEE) Staff publications (SWEE)

Efficient DNA walker guided by ordered cruciform-shaped DNA track for ultrasensitive and rapid electrochemical detection of lead ion

Zhu, Nuanfei

2024-03-20

Attribution 4.0 International

Zhu N, Wang K, Xiong D, et al., (2024) Efficient DNA walker guided by ordered cruciform-shaped DNA track for ultrasensitive and rapid electrochemical detection of lead ion. Analytica Chimica Acta, Volume 1302, May 2024, Article number 342492

https://doi.org/10.1016/j.aca.2024.342492

Downloaded from CERES Research Repository, Cranfield University